Energy & Environmental Science

Codesign of an Integrated Metal-Insulator-Semiconductor Photocathode for Photoelectrochemical Reduction of CO2 to Ethylene

Journal:	*Energy & Environmental Science*
Manuscript ID	EE-ART-10-2022-003525.R2
Article Type:	Paper
Date Submitted by the Author:	19-May-2023
Complete List of Authors:	Kim, Chanyeon; Daegu Gyeongbuk Institute of Science & Technology King, Alex; University of California Berkeley, Chemical and Biomolecular Engineering Aloni, Shaul; Lawrence Berkeley National Laboratory, The Molecular Foundry Toma, Francesca Maria; Lawrence Berkeley National Lab, Joint center for Artificial Photosynthesis Weber, Adam; Lawrence Berkeley National Laboratory, Energy Technologies Area Bell, Alexis; University of California, Chemical and Biomolecular Engineering

Broader Context Statement

The climate crisis resulting from the accumulation of atmospheric CO_2 has motivated growing interest in the conversion of CO_2 to fuels and chemicals using renewable sources of energy (*e.g.*, wind and solar radiation). One approach for doing so is photoelectrochemical carbon dioxide reduction (PEC CO_2R), a process that can directly reduce CO_2 to useful compounds using only water and sunlight. If CO_2 can be captured from the atmosphere, such a process could provide a sustainable source of carbon-based fuels. To date, however, the design principles for successful integration of light absorption, charge separation, and catalyst components of a PEC device are not well understood. This work investigates the co-design of a metal-insulator-semiconductor (MIS) photocathode/catalyst system with the aim of demonstrating how the system elements should be chosen in order to achieve a high selectivity and current density to ethylene via PEC CO_2R. The knowledge gained here also provides insights directly applicable to other PEC systems.

Codesign of an Integrated Metal-Insulator-Semiconductor Photocathode for Photoelectrochemical Reduction of CO_2 to Ethylene

Chanyeon Kim[1,2,3,6], Alex J. King[1,2,3], Shaul Aloni[2,4], Francesca M. Toma[2,3], Adam Z. Weber[2,5], and Alexis T. Bell[1,2,3]*

[1]Department of Chemical and Biomolecular Engineering, University of California, Berkeley, California 94720.

[2]Liquid Sunlight Alliance, Lawrence Berkeley National Laboratory, Berkeley, California 94720.

[3]Chemical Sciences Division, Lawrence Berkeley National Laboratory, Berkeley, California 94720.

[4]The Molecular Foundry, Lawrence Berkeley National Laboratory, Berkeley, California 94720.

[5]Energy Technologies Area, Lawrence Berkeley National Laboratory, Berkeley, California 94720.

[6]Department of Energy Science & Engineering, Daegu Gyeongbuk Institute of Science and Technology, Daegu 42988, Republic of Korea

*Correspondence to: alexbell@berkeley.edu (A.T. Bell)

Abstract

Photoelectrochemical carbon-dioxide reduction (PEC CO_2R) is a potentially attractive means for producing chemicals and fuels using sunlight, water, and carbon dioxide; however, this technology is in its infancy. To date, most studies of PEC CO_2R have reported products containing one carbon atom (C_1 products) but the production of valuable products containing two or more carbons (C_{2+} products), such as ethylene, ethanol, etc., is rarely demonstrated. Metal-semiconductor-insulator (MIS) photocathode/catalyst structures offers a promising approach for this purpose, since they integrate the functions of light absorption, charge separation, and catalysis. In this study, we have investigated a Cu/TiO_2/p-Si photocathode/catalyst structure with the aim of establishing the effects of semiconductor-insulator interactions on the performance of the photocathode and the influence of the direction of illumination of the MIS structure on the total current density and the distribution of products formed by on the Cu catalyst. We have also examined the influence of ionomer coatings deposited on the Cu surface on the total current density and the distribution of products formed. A major finding is that for a fixed Cu potential the distribution of products formed by PEC CO_2R are the same, irrespective of the direction of illumination, and are identical to those obtained by electrochemical reduction of CO_2 (EC CO_2R). Another important finding is that the total current density and the faradaic efficiency to ethylene are enhanced significantly by deposition of a thin bilayer of Sustainion/Nafion onto the surface of the Cu.

Broader Context

The climate crisis resulting from the accumulation of atmospheric CO_2 has motivated growing interest in the conversion of CO_2 to fuels and chemicals using renewable sources of energy (*e.g.*, wind and solar radiation). One approach for doing so is photoelectrochemical carbon dioxide reduction (PEC CO_2R), a process that can directly reduce CO_2 to useful compounds using only water and sunlight. If CO_2 can be captured from the atmosphere, such a process could provide a sustainable source of carbon-

based fuels. To date, however, the design principles for successful integration of light absorption, charge separation, and catalyst components of a PEC device are not well understood. This work investigates the co-design of a metal-insulator-semiconductor (MIS) photocathode/catalyst system with the aim of demonstrating how the system elements should be chosen in order to achieve a high selectivity and current density to ethylene via PEC CO_2R. The knowledge gained here also provides insights directly applicable to other PEC systems.

Introduction

Solar production of carbon-containing fuels envisions the direct conversion of solar radiation, carbon dioxide, and water to produce gaseous or liquid fuels.[1-4] This idea is particularly attractive if the carbon dioxide can be sourced from the atmosphere, since it would enable a circular carbon economy. Most previous studies of PEC CO_2R have demonstrated only small amounts of C_1 products, such as CO, CH_4, HCOOH, etc.[5-7], rather than more valuable multi-carbon (C_{2+}) products.[8, 9] Therefore, it is important to develop a fundamental understanding of how the interplay between the components of a PEC CO_2R photocathode/catalyst structure interact, and how these interactions can be best utilized to achieve high yields of products such as C_2H_4 and C_2H_5OH. These products are targeted because they can be converted to higher molecular weight, preferably liquid, hydrocarbons and alcohols that have high volumetric and mass energy densities.[8, 10, 11]

A key challenge for the development of a PEC CO_2R system is the susceptibility of most photo-absorbers to chemical corrosion and photodegradation in the presence of an electrolyte.[5-7, 12, 13] Moreover, the best photocathodes are poor catalysts for the reduction of CO_2.[13, 14] These issues have led researchers to explore metal-insulator-semiconductor (MIS) structures as photocathodes.[15-20] The metal layer improves reaction kinetics by lowering the overpotential required to achieve a given current density.[14] Photocathode degradation can be inhibited by covering the surface of the semiconductor with a very thin, corrosion-resistant, insulating layer, such as a metal oxide.[17] The insulating layer also serves as a carrier-selective tunneling contact, which helps to mitigate carrier recombination in the metal layer and improve product formation rates. The role of the protective (insulating) layer in MIS structures has recently been explored for PEC water splitting;[16, 18, 21-23] however, in most studies of PEC CO_2R, the role of the insulating film has been underexplored and limited to its effect as a passivation layer.[19, 24, 25] We note further that MIS structures have great potential for PEC CO_2R to C_{2+} products if the semiconductor, insulating layer, and catalyst material can be selected and adapted to each other (*i.e.*, co-designed) to achieve high photovoltage and current, as well as a high faradaic efficiency to

ethylene.[19-21, 24]

The reaction microenvironment near the catalyst surface is also vitally important. Extensive studies have revealed that Cu-based catalysts are best suited for the formation of C_{2+} products[26-28] and that the morphology of the Cu surface, electrolyte cation identity, and the local pH of the electrolyte in contact with the catalyst surface influence both its activity and selectivity for CO_2R.[29-31] Recent work has also demonstrated that the activity and selectivity of Cu for producing C_{2+} products can be enhanced significantly by using thin ionomer films in order to enhance the pH and the CO_2/H_2O ratio at the catalyst surface.[30] A further question is whether an MIS structure using Cu as the catalyst should be illuminated from its dry-side or its wet-side, the side in contact with the electrolyte. Prior work on PEC water splitting has shown that dry-side and wet-side illumination can produce differences in the transfer and utilization of absorbed light energy.[32, 33]

The aim of the present study was to understand how the semiconductor-insulator interactions in an MIS structure affect the photovoltage and photocurrent available to drive PEC CO_2R. To this end, we conducted a systematic investigation of the role of each component in a Cu/TiO_2/p-Si MIS structure. Because of the close interactions of the different elements of an MIS structure, it is useful to first identify the relationships among the elements, which are illustrated in Figure 1. The semiconductor light absorber is p-doped silicon (p-Si), a commonly available material that has been investigated previously for PEC applications. Cu catalyst was chosen as the catalyst because it exhibits the ability to catalyze the electrochemical reduction of CO_2 to C_{2+} products with high faradaic efficiency.[26-28] TiO_2 was used as the protective layer for p-Si because it is known to be stable in aqueous electrolytes.[17, 34] Figure 1 also shows that TiO_2 and p-Si have a low conduction band offset and a large valence band offset.[35] These are important characteristics for achieving carrier selective tunneling, which is exponentially dependent on the band offset between the semiconductor and insulator. A larger band offset results in a lower tunneling probability and, consequentially, a lower rate of carrier tunneling. Thus, a TiO_2 insulating layer is well suited for protecting the semiconductor and enabling facile tunneling of the

desired charge (electrons) due to its high tunneling probability. The tunneling probability is also exponentially dependent on the thickness of the insulator; hence, the TiO_2 layer must be thin enough to allow electron tunneling through it to the metal layer, but thick enough to protect the semiconductor and limit hole tunneling.[36-38] Therefore, an optimum TiO_2 thickness is expected in order to achieve high photovoltages.[15, 17] We note that an understanding of how the thickness of the TiO_2 layer alters the environment at the semiconductor surface, and, subsequently, the photovoltage, is not currently known.

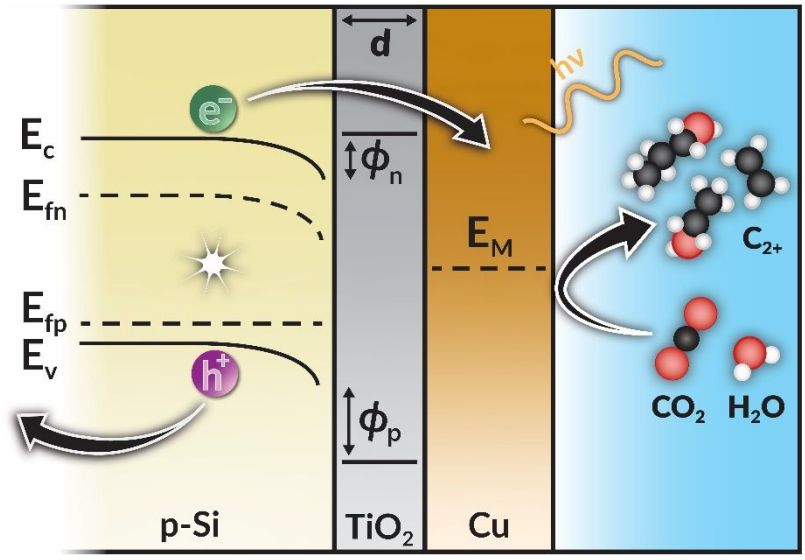

Figure 1. Band diagram illustration of an MIS photocathode converting CO_2 to C_2 products. Electrons can easily tunnel into the Cu layer because of the small barrier (ϕ_n), whereas hole tunneling is blocked by the large barrier (ϕ_p). d is the thickness of the TiO_2 layer. E_c and E_v are the conduction and valence bands, respectively. E_{fn}, E_{fp}, and E_M are the electron and hole quasi-Fermi level, respectively, and the metal Fermi level.

Results and Discussion

The effects of each component of a Cu/TiO_2/p-Si MIS structure on the total current density, photovoltage, and product Faradaic efficiencies for PEC CO_2R

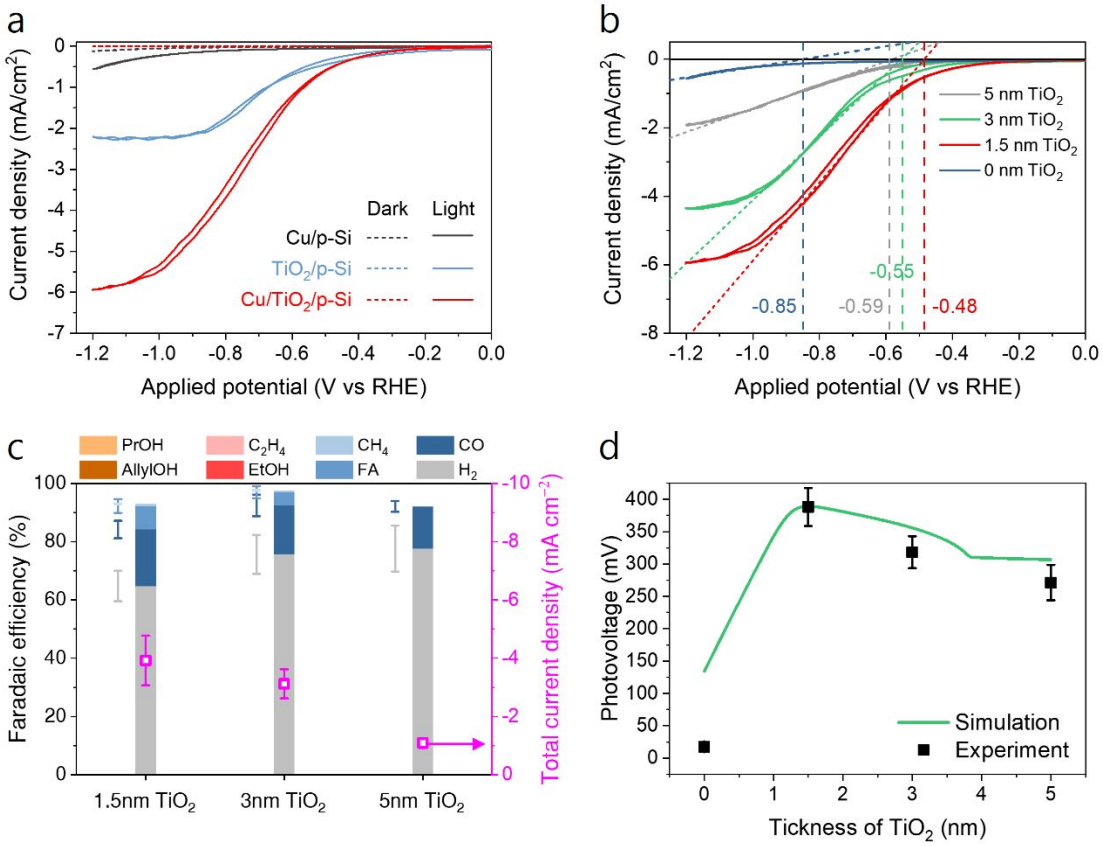

Figure 2. The effect and role of each component in the MIS photocathode. a. response in photocurrent during CV using various configurations of photocathode in CO_2R environments under dry-side illumination, b. photocurrent obtained during CV, c. product distribution obtained during CA at –0.9 V vs RHE, and d. comparison of the theoretical and experimentally measured photovoltage with respect to the thickness of TiO_2 insulator layer in in Cu/TiO_2/p-Si MIS photocathode at zero current density. In a-c, PEC CO_2R was conducted in the presence of 0.1 M $CsHCO_3$ electrolyte.

Figure 2 illustrates the effect of each component comprising the MIS photocathode on the current density for a given applied voltage. Cyclovoltammetry (CV) data were collected using a compression cell with two symmetric anodic chambers placed perpendicular to the cathode chamber (see Figure 3a, below)[39] for different photocathode configurations under conditions of no illumination (dark) and dry-side illumination (Figure 2a), *i.e.*, the side that is not exposed to the electrolyte (also referred elsewhere as back-side). We note that bare p-Si has been previously shown to be a poor CO_2R catalyst and primarily evolves H_2;[14] hence, our investigation first examined Cu on p-type silicon (Cu/p-

Si), to improve CO_2R activity. Cu/p-Si exhibited only a slight increase in total current density (photocurrent) under dry-side illumination, denoted by the black solid line, compared to that obtained under dark conditions (dark current), denoted by dotted black line. This minor increase in current density under dry-side illumination is due to significant Fermi-level pinning of Cu and p-Si.[36-38]

When a thin layer of TiO_2 is used to passivate p-Si (TiO_2/p-Si), the photocurrent increases noticeably (blue solid line) due to improved carrier transport and defect-passivation of the insulating TiO_2 layer, whereas the dark current is similar to that obtained for Cu/p-Si. The principal product for TiO_2/p-Si, however, is H_2 (Figure S1). Interestingly, the photocurrent can be further increased with an additional Cu layer (Cu/TiO_2/p-Si MIS, red line) due to the increase in CO_2R activity relative to that for TiO_2/p-Si. These observations clearly demonstrate the role of each component. Although the TiO_2 layer only produces H_2, it enhances the photocurrent and photovoltage obtained from p-Si as a consequence of its effects on carrier tunneling and surface passivation. The effect of the TiO_2 layer can be varied by changing its thickness, which in turn affects the carrier-tunneling probabilities.[16, 18, 21] As the TiO_2 layer thickness decreases from 5 nm, not only the photocurrent but also the photovoltage increases. The photovoltage was estimated by the shift in potential at which current flow begins (the onset potential) for each MIS photocathode (Figure 2b) and that for electrochemical (EC) CO_2R (Figure S2). The differences in PEC CO_2R performances during chronoamperometry (CA) at – 0.9 V vs RHE observed with varying TiO_2 thickness, shown in Figure 2c, is a consequence of differences in generated photovoltages. Our measurements, shown in Figure 2d, indicate a TiO_2 thickness of ~ 1.5 nm leads to the highest photovoltage (~ 400 mV).

The effects of TiO_2 thickness on the photovoltage for the Cu/TiO_2/p-Si photocathode structure was modeled in order to explain why a maximum in the photovoltage occurs at a particular insulator thickness. An overview of this effort is presented in the Supporting Information; specific details can be found elsewhere.[40] This work reveals that with increasing insulator thickness, the electron-tunneling probability decreases (Figure S3) due to an attenuation of the electron wavefunction. The lowered tunneling probability increases the resistances to electron transport across the MIS interface, which, in

turn, leads to a buildup of electrons near the semiconductor surface. This buildup of electrons occurs for TiO_2 thicknesses $\lesssim 1.5$ nm, beyond which the electron concentration decreases; see Figure S4. This decrease in electron concentration occurs because of a high bulk and interfacial recombination rate, as seen in Figure S5, which is attributable to the large electron concentration and density of interfacial trap sites. The electron concentration at the semiconductor surface alters the quasi-Fermi level of electrons, and, consequentially, the photovoltage (for details the reader is referred to the Supporting Information and Figure S4); the band energy diagram at varying TiO2 thicknesses is shown in Figure S6. Thus, the increase in photovoltage for TiO_2 films $\lesssim 1.5$ nm thick is due to the increase in electron concentration, whereas the decrease in electron concentration for TiO_2 thicknesses > 1.5 nm causes the reduction in photovoltage. We note that the effects of quantum confinement in the TiO_2 layer on the simulation results are negligible, as shown in Figure S7. Notwithstanding the discrepancies observed in the absence of a TiO_2 layer and for thick TiO_2 layers, Figure 2d shows that the theoretical predictions capture the experimental trends in photovoltage with insulator thickness quite effectively, especially at thicknesses relevant to this study.

The effects of dry-side vs wet-side illuminations on the performance of a Cu/TiO_2/p-Si MIS structure

The MIS architecture of the photocathode is geometrically asymmetric; therefore, the questions arises whether the performance of the MIS structure will differ when it is illuminated from the dry- vs the wet-side. This question was investigated using the compression cell shown in Figure 3a (see the Experimental Methods section for more details).[39] To evaluate the effect of light in terms of the electric potential at the Cu surface, where CO_2R occurs, an electric contact was made on the wet-side as well as through an Al/Au ohmic contact located on the dry-side of the MIS photocathode (see Figure 3b). Prior to using the MIS photocathode for PEC CO_2R under wet-side illumination, the light transmission through the Cu and TiO_2 layers was measured. As shown in Figure S8a, incident light transmission through 1.5 nm of TiO_2 was > 90 % for wavelengths from 350 to 1500 nm. However,

when a Cu layer was deposited on top of the TiO_2 layer, light transmission decreased noticeably from < 80 % to below 55 % as the thickness of the Cu layer increased from 10 to 25 nm. As shown in Figure S8b, a decrease in light transmission leads to a decrease in the photocurrent. When the Cu thickness was 10 nm, the hydrogen evolution reaction (HER) dominated over CO_2R, most likely due to partial exposure of the TiO_2 layer below the Cu. These results indicate that a Cu thickness of 15 nm is optimal in order to reduce the loss of light transmission, while concurrently promoting CO_2R selectivity; hence, 15 nm was used in all subsequent experiments.

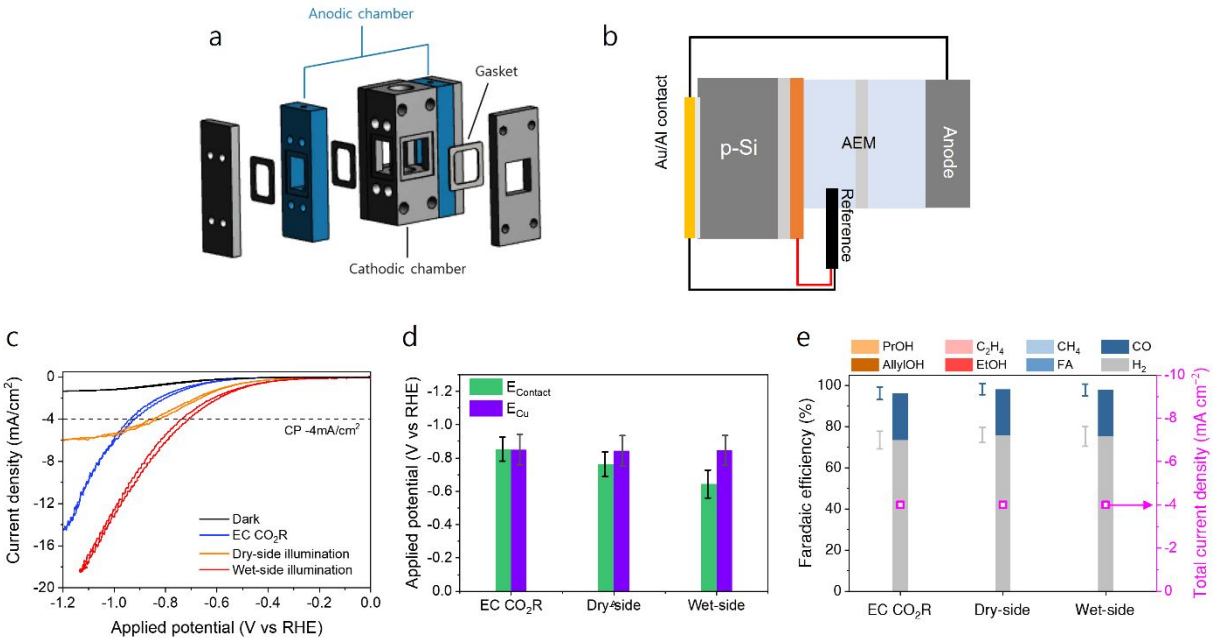

Figure 3. PEC CO_2R using MIS photocathode under dry-side and wet-side illuminations. Schematic illustration of **a.** PEC cell enabling both dry-side and wet-side illumination and **b.** configuration of electric circuit. **c.** CV curves obtained using MIS photocathode under various conditions of EC CO_2R, dark, dry-side and wet-side illumination. Effect of illuminating direction on **d.** potential measured at Cu surface and **e.** product distribution during PEC CO_2R using MIS photocathode at constant current density of – 4mA/cm^2. In **c-e**, PEC CO_2R was conducted in the presence of 0.1 M $CsHCO_3$ electrolyte.

Under dry-side illumination the photovoltage and photocurrent is generated solely by light absorption from p-Si; under wet-side illumination, however, the light passes through all three layers (Cu, TiO_2, and p-Si). Therefore, the effect of light with respect to the direction of illumination needs to be investigated in terms of both photocurrent and photovoltage in order to ascertain the effects of light absorption and reflection by the Cu and TiO_2 layers. Figure 3c shows CV data acquired for dry-side and

wet-side illumination of the MIS photocathode/catalyst as well as for EC CO_2R, which use identical Cu catalysts. In the case of EC CO_2R, the potential was applied between the Cu surface in MIS photocathode/catalyst and the reference electrode using a potentiostat. Interestingly, the photocurrent obtained under wet-side illumination (red line) was noticeably higher than that obtained under dry-side illumination (orange line), even though partial light absorption and reflection by the Cu and TiO_2 layers occurred in the latter case. This observation implies there is better utilization of absorbed photons under wet-side illumination compared to dry-side illumination. To validate this hypothesis, a potential was applied to the p-Si (at the Au/Al contact on the dry-side) and the potential at the Cu layer on the wet-side was measured during chronopotentiometry (CP) at – 4 mA/cm^2 (Figure 3d). While the potential measured at the Cu surface was identical for all cases (purple columns), there were differences in the potential applied by the potentiostat, indicating that the electric potential required to reach – 4 mA/cm^2 was different for EC CO_2R and PEC CO_2R under dry-side and wet-side illumination (green columns). The required applied potential to reach a current density of – 4mA/cm^2 was – 0.76 V and – 0.64 V vs RHE for dry-side and wet-side illumination, respectively. The additional 120 mV of photovoltage under wet-side illumination compared to dry-side illumination is a result of the improved charge utilization. For a nearly identical potential at the Cu surface, around – 0.84 V vs RHE, the product distributions obtained for EC CO_2R and PEC CO_2R under wet-side and dry-side illumination were nearly identical (Figure 3e).

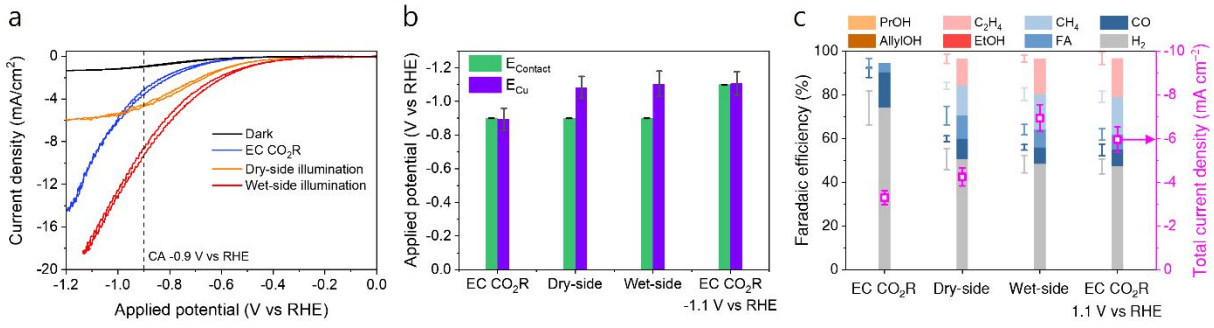

Figure 4. PEC CO_2R using MIS photocathode under dry-side and wet-side illuminations at constant potential condition of –0.9 V vs RHE. a. CV curves obtained using MIS photocathode under various conditions of EC CO_2R, dark, dry-side and wet-side illumination. Effect of illuminating direction on **b.** potential measured

at Cu surface under the constant applied potential of -0.9V vs RHE to p-Si with respect to the reference electrode and **c.** product distribution. In **a-c**, PEC CO_2R was conducted in the presence of 0.1 M $CsHCO_3$ electrolyte.

The effects of dry-side and wet-side illumination were also investigated at a constant applied potential of – 0.9 V vs RHE, shown in Figure 4a in order to further support our hypothesis of enhanced charge utilization under wet-side illumination. Although the potential applied by the potentiostat (green columns) was the same, the potential at the Cu surface decreased from – 0.89 to – 1.07 to – 1.10 V vs RHE for EC CO_2R, PEC CO_2R under dry-side illumination, and PEC CO_2R under wet-side illumination, respectively (Figure 4b). As a consequence of the larger negative potential at the Cu surface, PEC CO_2R under dry-side and wet-side illumination exhibited increased current density for CO_2R vs HER and, more importantly, formation of ethylene. When the potential at the Cu surface was similar for PEC CO_2R under wet-side illumination and EC CO_2R (– 1.10 V vs RHE), the product faradaic efficiencies were similar as well (Figure 4c). Thus, the effect of light is to reduce the potential required by the potentiostat to maintain the Cu potential around – 1.10 V vs RHE. It is important to note that PEC CO_2R under dry-side illumination produced a saturated current response, reaching a plateau at around – 7 mA/cm^2 at – 1.2 V vs RHE as shown in Figure 4a. This plateau in current density is not related to either mass-transport-limited CO_2R or tunneling resistances of photo-generated charges through the TiO_2 layer because these limitations would also been seen in EC CO_2R and PEC CO_2R under wet-side illumination, respectively. Therefore, saturation of the photocurrent under dry-side illumination is attributed to carrier recombination across the p-Si layer.

Similar limitations from carrier recombination has been reported for PEC water splitting.[32, 33, 41-43] In these studies, wet-side illumination resulted in several fold higher photocurrents than dry-side illumination, in agreement with the findings shown here. The authors of these studies proposed that the diffusion length of charge carriers, which is less than a micron, is much shorter than the thickness of the semiconductor photo-absorber, several hundred microns. Hence, a significant number of excited electrons recombine with holes as they travel across the photo-absorber to the metal surface, resulting in the low photocurrent observed under dry-side illumination. This interpretation is further supported

by the work of Bae *et al*., who investigated the influence of the thickness of a p^+pn^+-Si photo-absorber on the photocurrent produced during PEC water splitting under both wet-side and dry-side illumination.[32] They found that the photocurrent under dry-side illumination was ~ 20% lower than that under wet-side illumination even though the thickness of p^+pn^+-Si was reduced from 350 to 50 μm. The authors attributed this finding to the small ratio of carrier diffusion length to the thickness of the p^+pn^+-Si photo-absorber. Therefore, we conclude that dry-side illumination cannot achieve photocurrents as high as those attained under wet-side illumination unless the carrier diffusion length is improved.

Effects of ionomer coatings on the activity and product selectivity of Cu for PEC CO_2R

Previous studies of EC CO_2R have shown that the microenvironment near the surface of a Cu catalyst plays a critical role in defining its activity and selectivity for producing C_{2+} products. It has been found that a high pH and CO_2/H_2O ratio at the Cu surface promoted the formation of C_{2+} products relative to C_1 products and H_2.[29, 30] We have recently reported that these requirements can be met by coating the surface of Cu with a thin ionomer bilayer. For CO_2R on Nafion/Sustainion/Cu, the Sustainion layer, which is an anion conducting ionomer with high CO_2 affinity, enhances local CO_2 concentration near Cu surface; whereas, the Nafion layer, which is a cation conducting ionomer with a negative background charge, causes the accumulation of OH^- through Donnan exclusion.[30]

We investigated the effects depositing an ionomer bilayer (Nafion on top of Sustainion) on the surface of Cu in a Cu/TiO_2/p-Si MIS structure to see whether the bilayer would enhance the formation of C_{2+} products formed by PEC CO_2R. The loading of each ionomer layer was selected on the basis of the experiments described in the Supporting Information (See Figure S9). The optimal loadings of Nafion on Sustainion/MIS (N/S/MIS) were chosen to be 0.9 μg/cm^2 and 1.8 μg/cm^2, respectively. As seen in in Figure 5a, the N/S/MIS configuration produced a higher photocurrent than that obtained for the uncoated MIS, even though the light flux to the photocathode was 10% lower due to light absorption by the ionomer bilayer (Figure S10). To further investigate the influence of the ionomer coatings on the product distribution, CA was conducted at – 0.9 V vs RHE under wet-side illumination. Similar to our

previous results, the potential at the Cu surface was about 0.2 V more negative than that applied to the MIS (Figure 5b), which is comparable to the value obtained using the uncoated MIS structure under dry-side and wet-side illuminations. However, due to the high local pH caused by Donnan exclusion from the presence of the Nafion layer, the selectivity to hydrogen and methane, which are pH sensitive products,[44-46] decreased. Concurrently, the total current density increased up to 10 mA/cm^2 because of the high local CO_2 concentration in the Sustainion layer (Figure 5c). The impact of the bilayer ionomer film on MIS performance is more prominent in terms of partial current density because both selectivity and total current density increased. As shown in Figure 5d, PEC CO_2R using the MIS structure under wet-side illumination exhibited a CO_2R partial current density of – 3.1 mA/cm^2 of which the partial current density for ethylene is – 0.9 mA/cm^2. These values increased to – 5.4 mA/cm^2 and – 2.3 mA/cm^2, respectively, by inclusion addition of the ionomer bilayer on Cu catalyst surface. This selectivity towards ethylene is maintained for several hours under sequential dark and illumination conditions, as shown in Figure S11. These observations are notable because EC CO_2R produced a partial current density for CO_2R of only – 0.6 mA/cm^2 without any ethylene formation at an applied potential of – 0.9 V vs RHE.

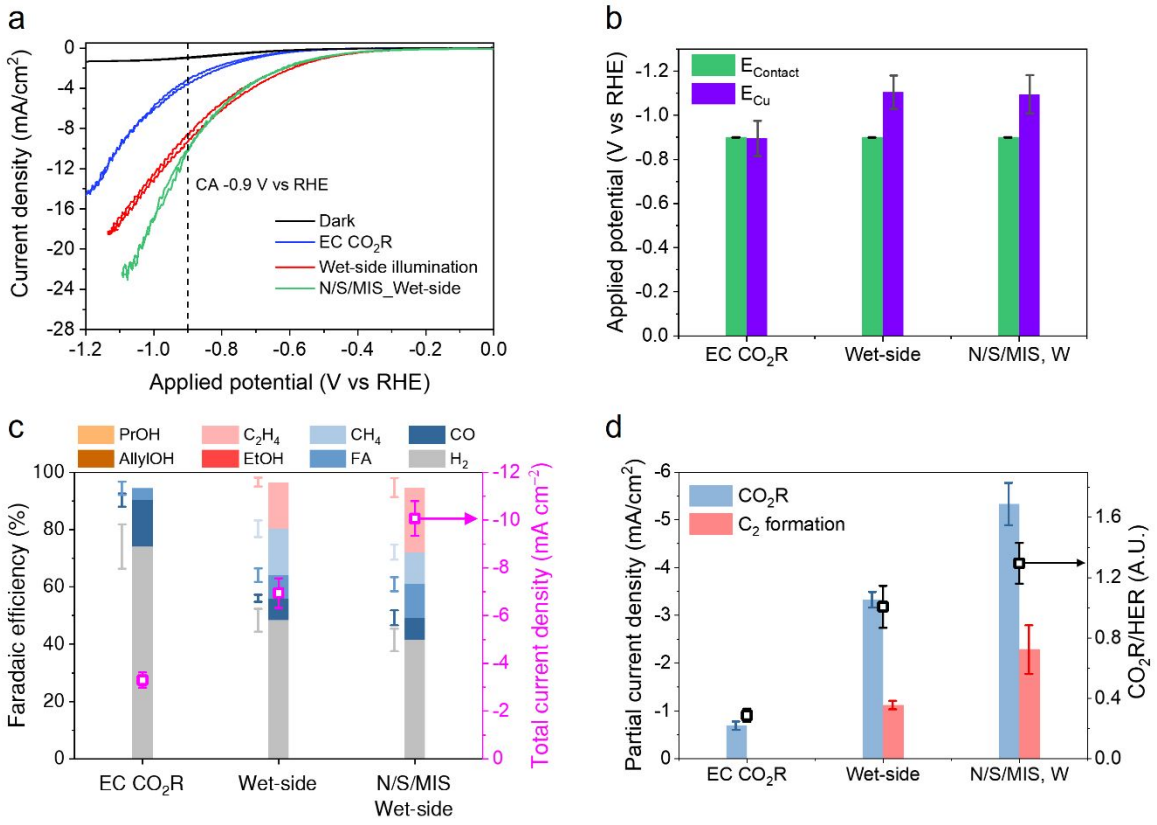

Figure 5. Effect of ionomer bilayer on PEC CO_2R using MIS photocathode. a. Comparison of CV curve obtained using N/S/MIS photocathode with those obtained using pristine MIS under various conditions. **b.** potential measured at Cu surface, **c.** product distribution, and **d.** partial current density for CO_2R and ethylene production during CA –0.9V vs RHE. All the PEC CO_2R was conducted in the presence of 0.1 M $CsHCO_3$ electrolyte.

Conclusions

The present study clearly demonstrates that the performance of a metal-insulator-semiconductor (MIS) photocathode/catalyst structure used for PEC CO_2 in CO_2-saturated 0.1 M $CsHCO_3$ can be tuned by altering the interface between the semiconductor and insulator layers, as well as by the direction of illumination. A thin TiO_2 layer deposited on p-Si improves the photocurrent and photovoltage obtained from the photocathode. This improvement occurs because of a moderate tunneling resistance through the insulating (TiO_2) film, which, in turn, causes a buildup of electrons at the p-Si surface that increases its quasi-Fermi level. Although wet-side illumination of a Cu/TiO_2/p-Si MIS photocathode attenuates the flux of light to the photo-absorber, a thin Cu layer (~ 15 nm) deposited

over the insulator exhibits a substantial increase in the photocurrent relative to dry-side illumination. The observed advantage of wet-side over dry-side illumination is a direct consequence of the low diffusion length of the excited charge carriers, leading to significant carrier recombination; this limits the collection of electrons at the Cu catalyst that subsequently drives CO_2R. The partial current density for CO_2R and that for ethylene production on Cu can be further enhanced by deposition of thin layers of Sustainion and then Nafion over the Cu surface. The bilayer coating increases the partial current for CO_2R, due to the higher solubility of CO_2 in the Sustanion layer, and increases the selectivity to ethylene, due to OH^- exclusion by the Nafion layer, which suppresses the formation of H_2. Under wet-side illumination, the net effect of the ionomer bilayer is that the partial current density of CO_2R is 2.5 times higher and that for ethylene is 4 times higher than that obtained by dry-side illumination of the Cu/TiO_2/p-Si MIS photocathode/catalyst structure in the absence of the bilayer coating. The fundamental knowledge gained from the present work can be applied directly to other combinations of metals, insulators, and semiconductors in order to facilitate the unbiased operation of PEC CO_2R for the production of C_{2+} products, as well as other photo-electrosynthetic processes.

Experimental Methods

Preparation of a Cu/TiO_2/p-Si MIS photocathode

Prior to fabricating an MIS photocathode, a 1-10 Ω-cm p-type silicon wafer (boron doped, 500μm thickness, <100> orientation, University Wafer Inc.) was rinsed consecutively with acetone (≥99.5%, VWR), isopropyl alcohol (Sigma Aldrich, 99.9%), and methanol (≥99.8%, VWR) for 30 min each. The p-Si wafer was then immersed in 1% HF for 5min to remove the native oxide layer and rinsed with Milli-Q water (18.2MΩ·cm). To make an ohmic contact with the p-Si wafer, it was masked with 2-mm wide Kapton tape in order to produce 1 mm of spacings between fingers. Al (99.999% Kurt J. Lesker) and Au (99.999% Kurt J. Lesker) were then sputtered onto the unmasked portions of the wafer. using an AJA ATC Orion-5 magnetron sputtering system on the masked p-Si in order to achieve target thickness of 50 nm for Al and 300 nm for Au. The TiO_2 insulating layer was deposited by atomic layer

deposition (ALD) on the opposite side to the one with Al/Au contacts. In the ALD process, the deposition chamber was heated to 125℃ and Titanium isopropoxide (TTIP, 99.999% trace metals basis, Sigma-Aldrich) was pulsed into the reactor, to form a TiO_2 film, after which water vapor was pulsed into the reactor. This ALD cycle was repeated in order achieve the desired thickness of the insulator layer, with the thickness measured using ellipsometry (α-SE, J.A.Woollam Co., Inc.). After ALD deposition of TiO_2, Cu (99.999% Kurt J. Lesker) was sputtered for different deposition time to change the thickness of the deposited Cu film. For the EC experiments, 15 nm of Cu was sputtered onto p^+-Si at the same conditions as those used for the MIS samples.

Characterization of the MIS photocathode

Cross-sectional images of a fresh 15nm Cu/1.5nm TiO_2/Si sample were obtained with STEM and energy filtered STEM. The STEM image (Figure S12a) shows there are three distinct layers in the MIS sample, and the energy filtered STEM confirms the three layers are Cu on TiO_2 on Si (Figures S12b and c). We also note the presence of the native SiO_2 layer between Si and TiO_2. STEM energy dispersive x-ray spectroscopy (EDS) also confirms these results (Figure S13a and b). We also performed STEM-EDS of the ionomer-bilayer-coated MIS sample, which shows the presence of the Nafion and Sustanion on top of the MIS photocathode (Figure S14).

Coating of ionomer layer on MIS photocathode

Commercial Nafion (Chemours, 850g mol^{-1} equivalent weight (EW), 20wt% dispersion in 20wt% N-propanol aqueous solution), and Sustainion (Dioxide Materials, 5% in ethanol) were drop cast onto the Cu/TiO_2/p-Si MIS system. Stock solutions were prepared by diluting the ionomer solution with isopropyl alcohol (Sigma Aldrich, 99.9%). Prepared stock solutions were drop cast to achieve different loading loadings of ionomers and then dried at room temperature for 1h.

Photoelectrochemical CO_2 reduction

PEC CO_2R was performed in a flow-through compression cell shown in Figure 3a.[39] The cell has 3 electrodes – an MIS photocathode, an Ag/AgCl (filled with 3.4M KCl, Leak-Free, Innovative Instruments) reference electrode, and a platinum foil (99.995%, Sigma-Aldrich) counter electrode. The cell has two identical anode chambers located perpendicular to the cathode chamber. All cell components were machined from polyether ether ketone (PEEK). An anion membrane (Selemion AMV, AGC Engineering Co.) was placed in between the cathodic chamber and two anodic chambers. A 0.05M solution of Cs_2CO_3 (99.995%, Sigma-Aldrich) was prepared using Milli-Q water and pretreated to remove metal impurities using chelating agent solution (Chelex 100, Na form, Sigma-Aldrich) prior to being used. The electrolyte was saturated with a flow of CO_2 (20 sccm, 99.999%, Praxair Inc) for 30 min in a gas-tight reservoir to obtain 0.1M of $CsHCO_3$ and circulated through the PEC cell using a peristaltic pump (FH100M, Thermo Scientific) at a rate of 80 ml min^{-1}. A solar simulator was used as the light source (300W, 1.5 A.M., 16S-Series, Solar Light) to obtain a light flux of 100 mW cm^{-2}. The desired flux was achieved by controlling the distance from the light source to the cell and by measuring the local flux using a radiometer (PMA2100, Solar Light). The illuminated area of the MIS photocathode was 1 cm^2 under both dry-side and wet-side illuminations. Electrochemical measurements were performed using a potentiostat (VSP-300, Biologic). An uncompensated resistance (R_u) was determined by both potentiostatic electrochemical impedance spectroscopy (PEIS) and the current interrupt (CI) method and compensated to 85% using the potentiostat. All potentials are shown after conversion to the RHE scale as $E_{RHE} = E_{Ag/AgCl} + 0.197\,V + 0.0591 \times pH$.

Product analysis

Gaseous products formed by PEC CO_2R were separated from liquid electrolysis in a gas-tight reservoir and then analyzed by online gas chromatograph (GC) using a gas chromatograph (7890B, Agilent) equipped with a pulsed-discharge helium ionization detector (PDHID) and ShinCarbon ST and Hayesep-Q capillary columns (Agilent); helium (99.9999%, Praxair Inc.) was used as the carrier gas. For quantitative analysis, a calibration curve for each gaseous product was generated by measuring the

signal for each component obtained by analysis of a series of NIST-traceable standard gas mixtures (100 to 8000 ppm, Airgas Inc.). Liquid products collected in the catholyte reservoir over a period of 30 min were analyzed in a high-pressure liquid chromatograph (HPLC) (UltiMate 3000, Thermo Scientific) equipped with Aminex HPX 87-H columns (Bio-Rad Inc.) and a refractive index detector (RID). The signal for each liquid product was quantified using a calibration curve based on a series of standard solutions for each product in the range of concentration from 0.1 to 20 mM. Faradaic efficiency (FE) corresponding to product *i* was calculated as $FE = \frac{nFc_iV}{I_{total}} \times 100\ \%$, where *n* is the number of electrons transferred, *F* is Faraday's constant, c_i is molar concentration of species *i*, *V* is the total volumetric flow rate and I_{total} is the measured total current.

Data availability

All data of this study is available within the article and its Supplementary Information.

Acknowledgments

This work was supported by the Liquid Sunlight Alliance, which is supported by the U.S. Department of Energy, Office of Science, Office of Basic Energy Sciences, Fuels from Sunlight Hub under Award Number DE-SC0021266 and Basic Science Research Program through the National Research Foundation of Korea (NRF) funded by the Ministry of Education (NRF-2021R1A6A3A14044966). A.J.K. acknowledges funding from the National Science Foundation Graduate Research Fellowship under Grant No. DGE 2146752. The authors acknowledge Finn Babbe for his help with characterizing the MIS sample, as well as the Molecular Foundry at Lawrence Berkeley National Laboratory for providing the necessary instrumentation.

Author contributions

C.K. performed photocathode preparation, photoelectrochemical experiments, characterizations, and data interpretation. A.J.K. performed theoretical calculations. S.A. conducted chemical and physical characterization of the MIS sample. A.T.B., A.Z.W., and F.M.T. supervised the project. All authors discussed the result and participated in the preparation of the manuscript.

Competing interests

Authors declare no competing interests.

References

1. W.-H. Cheng, A. de la Calle, H. A. Atwater, E. B. Stechel and C. Xiang, *ACS Energy Lett.*, 2021, **6**, 3096-3113.
2. A. J. King, J. C. Bui, A. T. Bell and A. Z. Weber, *ACS Energy Lett.*, 2022, DOI: 10.1021/acsenergylett.2c01041, 2694-2700.
3. G. Segev, J. Kibsgaard, C. Hahn, Z. J. Xu, W.-H. Cheng, T. G. Deutsch, C. Xiang, J. Z. Zhang, L. Hammarström, D. G. Nocera, A. Z. Weber, P. Agbo, T. Hisatomi, F. E. Osterloh, K. Domen, F. F. Abdi, S. Haussener, D. J. Miller, S. Ardo, P. C. McIntyre, T. Hannappel, S. Hu, H. Atwater, J. M. Gregoire, M. Z. Ertem, I. D. Sharp, K.-S. Choi, J. S. Lee, O. Ishitani, J. W. Ager, R. R. Prabhakar, A. T. Bell, S. W. Boettcher, K. Vincent, K. Takanabe, V. Artero, R. Napier, B. R. Cuenya, M. T. M. Koper, R. Van De Krol and F. Houle, *J. Phys. D: Appl. Phys.*, 2022, **55**, 323003.
4. Q. Wang, C. Pornrungroj, S. Linley and E. Reisner, *Nat. Energy*, 2022, **7**, 13-24.
5. J. He and C. Janáky, *ACS Energy Lett.*, 2020, **5**, 1996-2014.
6. V. Kumaravel, J. Bartlett and S. C. Pillai, *ACS Energy Lett.*, 2020, **5**, 486-519.
7. Y. Liu and L. Guo, *J. Chem. Phys.*, 2020, **152**, 100901.
8. S. Nitopi, E. Bertheussen, S. B. Scott, X. Liu, A. K. Engstfeld, S. Horch, B. Seger, I. E. L. Stephens, K. Chan, C. Hahn, J. K. Nørskov, T. F. Jaramillo and I. Chorkendorff, *Chem. Rev.*, 2019, **119**, 7610-7672.
9. W. Lai, Y. Qiao, J. Zhang, Z. Lin and H. Huang, *Energy Environ. Sci.*, 2022, **15**, 3603-3629.
10. S. Verma, B. Kim, H.-R. M. Jhong, S. Ma and P. J. A. Kenis, *ChemSusChem*, 2016, **9**, 1972-1979.
11. D. T. Whipple and P. J. A. Kenis, *J. Phys. Chem. Lett.*, 2010, **1**, 3451-3458.
12. G. Liu, F. Zheng, J. Li, G. Zeng, Y. Ye, D. M. Larson, J. Yano, E. J. Crumlin, J. W. Ager, L.-w. Wang and F. M. Toma, *Nat. Energy*, 2021, **6**, 1124-1132.
13. A. K. Singh, J. H. Montoya, J. M. Gregoire and K. A. Persson, *Nat. Commun.*, 2019, **10**, 443.
14. R. Hinogami, Y. Nakamura, S. Yae and Y. Nakato, *J. Phys. Chem. B*, 1998, **102**, 974-980.
15. I. A. Digdaya, B. J. Trześniewski, G. W. P. Adhyaksa, E. C. Garnett and W. A. Smith, *J. Phys. Chem. C*, 2018, **122**, 5462-5471.
16. J. Hemmerling, J. Quinn and S. Linic, *Adv. Energy Mater.*, 2020, **10**, 1903354.
17. J. R. Hemmerling, A. Mathur and S. Linic, *Acc. Chem. Res.*, 2021, **54**, 1992-2002.
18. J. Quinn, J. Hemmerling and S. Linic, *ACS Energy Lett.*, 2019, **4**, 2632-2638.
19. P. Wen, H. Li, X. Ma, R. Lei, X. Wang, S. M. Geyer and Y. Qiu, *J. Mater. Chem. A*, 2021, **9**, 3589-3596.
20. T. Zhu and M. N. Chong, *Nano Energy*, 2015, **12**, 347-373.
21. I. A. Digdaya, G. W. P. Adhyaksa, B. J. Trześniewski, E. C. Garnett and W. A. Smith, *Nat.*

Commun., 2017, **8**, 15968.
22. S. Lee, L. Ji, A. C. De Palma and E. T. Yu, *Nat. Commun.*, 2021, **12**, 3982.
23. P. P. Sahoo, M. Mikolášek, K. Hušeková, E. Dobročka, J. Šoltýs, P. Ondrejka, M. Kemény, L. Harmatha, M. Mičušík and K. Fröhlich, *ACS Appl. Energy Mater.*, 2021, **4**, 11162-11172.
24. Gurudayal, J. W. Beeman, J. Bullock, H. Wang, J. Eichhorn, C. Towle, A. Javey, F. M. Toma, N. Mathews and J. W. Ager, *Energy Environ. Sci.*, 2019, **12**, 1068-1077.
25. S. Chu, P. Ou, P. Ghamari, S. Vanka, B. Zhou, I. Shih, J. Song and Z. Mi, *J. Am. Chem. Soc.*, 2018, **140**, 7869-7877.
26. A. Bagger, W. Ju, A. S. Varela, P. Strasser and J. Rossmeisl, *ChemPhysChem*, 2017, **18**, 3266-3273.
27. D. Gao, R. M. Arán-Ais, H. S. Jeon and B. Roldan Cuenya, *Nat. Catal.*, 2019, **2**, 198-210.
28. C. W. Lee, C. Kim and B. K. Min, *Nano Converg.*, 2019, **6**, 8.
29. J. C. Bui, C. Kim, A. J. King, O. Romiluyi, A. Kusoglu, A. Z. Weber and A. T. Bell, *Acc. Chem. Res.*, 2022, **55**, 484-494.
30. C. Kim, J. C. Bui, X. Luo, J. K. Cooper, A. Kusoglu, A. Z. Weber and A. T. Bell, *Nat. Energy*, 2021, **6**, 1026-1034.
31. C. Kim, L.-C. Weng and A. T. Bell, *ACS Catal.*, 2020, **10**, 12403-12413.
32. D. Bae, T. Pedersen, B. Seger, M. Malizia, A. Kuznetsov, O. Hansen, I. Chorkendorff and P. C. K. Vesborg, *Energy Environ. Sci.*, 2015, **8**, 650-660.
33. S. Wang, T. Wang, B. Liu, H. Li, S. Feng and J. Gong, *Natl. Sci. Rev.*, 2020, **8**.
34. J. Zhang, C. D. Sewell, H. Huang and Z. Lin, *Adv. Energy Mater.*, 2021, **11**, 2102767.
35. S. Avasthi, W. E. McClain, G. Man, A. Kahn, J. Schwartz and J. C. Sturm, *Appl. Phys. Lett.*, 2013, **102**, 203901.
36. A. Agrawal, J. Lin, M. Barth, R. White, B. Zheng, S. Chopra, S. Gupta, K. Wang, J. Gelatos, S. E. Mohney and S. Datta, *Appl. Phys. Lett.*, 2014, **104**, 112101.
37. D. Connelly, C. Faulkner, P. A. Clifton and D. E. Grupp, *Appl. Phys. Lett.*, 2006, **88**, 012105.
38. W. Mönch, *J. Appl. Phys.*, 2012, **111**, 073706.
39. O. J. Alley, K. Wyatt, M. A. Steiner, G. Liu, T. Kistler, G. Zeng, D. M. Larson, J. K. Cooper, J. L. Young, T. G. Deutsch and F. M. Toma, *Front. Energy Res.*, 2022, **10**, 884364.
40. A. J. King, A. Z. Weber and A. T. Bell, *ACS Applied Materials & Interfaces*, 2023, **15**, 23024-23039.
41. R. P. Antony, M. Zhang, K. Zhou, S. C. J. Loo, J. Barber and L. H. Wong, *ACS Omega*, 2018, **3**, 2724-2734.
42. P. S. Bassi, L. Xianglin, Y. Fang, J. S. C. Loo, J. Barber and L. H. Wong, *Phys. Chem. Chem. Phys.*, 2016, **18**, 30370-30378.
43. S. S. M. Bhat, S. A. Lee, J. M. Suh, S.-P. Hong and H. W. Jang, *Appl. Sci.*, 2018, **8**, 1765.
44. Y. Hori, R. Takahashi, Y. Yoshinami and A. Murata, *J. Phys. Chem. B*, 1997, **101**, 7075-7081.

45. X. Liu, P. Schlexer, J. Xiao, Y. Ji, L. Wang, R. B. Sandberg, M. Tang, K. S. Brown, H. Peng, S. Ringe, C. Hahn, T. F. Jaramillo, J. K. Nørskov and K. Chan, *Nat. Commun.*, 2019, **10**, 32.
46. L. Wang, S. A. Nitopi, E. Bertheussen, M. Orazov, C. G. Morales-Guio, X. Liu, D. C. Higgins, K. Chan, J. K. Nørskov, C. Hahn and T. F. Jaramillo, *ACS Catal.*, 2018, **8**, 7445-7454.